

Weighted Singular Value Thresholding and its Application to Background Estimation

Aritra Dutta

*Department of Mathematics
University of Central Florida
Orlando, FL 32816, USA*

D.ARITRA2010@KNIGHTS.UCF.EDU

Boqing Gong

*Center for Research in Computer Vision
University of Central Florida
Orlando, FL 32816-2365, USA*

BGONG@CRCV.UCF.EDU

Xin Li

*Department of Mathematics
University of Central Florida
Orlando, FL 32816, USA*

XIN.LI@UCF.EDU

Mubarak Shah

*Center for Research in Computer Vision
University of Central Florida
Orlando, FL 32816-2365, USA*

SHAH@CRCV.UCF.EDU

Abstract

Singular value thresholding (SVT) plays an important role in the well-known robust principal component analysis (RPCA) algorithms which have many applications in computer vision and recommendation systems. In this paper, we formulate and study a *weighted* singular value thresholding (WSVT) problem, which uses a combination of the nuclear norm and a weighted Frobenius norm. We present an algorithm to numerically solve WSVT and establish the convergence of the algorithm. As a proof of concept, we apply WSVT with a simple choice of weight learned from the data to the background estimation problem in computer vision. The numerical experiments show that our method can outperform RPCA algorithms. This indicates that instead of tackling the computationally expensive ℓ_1 norm employed in RPCA, one may switch to the weighted Frobenius norm and achieve about the same or even better performance.

Keywords: Singular value thresholding, weighted low-rank approximation, alternating direction method, robust principal component analysis, background estimation.

1. Introduction

The classical principal component analysis (PCA) problem (Eckart and Young, 1936; Jolliffe, 2002) can be defined as a best approximation to a given matrix $X \in R^{m \times n}$ by a rank r matrix under the Frobenius norm as follows:

$$\hat{B} = \arg \min_{\substack{B \\ r(B) \leq r}} \|X - B\|_F, \quad (1)$$

where $r(B)$ denotes the rank of the matrix B . If $U\Sigma V^T$ is a singular value decomposition (SVD) of X , then solutions to this problem are given by thresholding on the singular values of X : $\hat{B} = U\mathbf{H}_r(\Sigma)V^T$, where \mathbf{H}_r is the hard-thresholding operator that keeps the r largest singular values and replaces the others by 0.

As it turns out, the nuclear norm $\|B\|_*$, the sum of the singular values of B , is a good substitution for $r(B)$ in many problems (Candès and Plan, 2009). Cai et al. (2010), used this to propose the following unconstrained convex optimization formulation of a low rank approximation problem:

$$\hat{B} = \arg \min_B \left\{ \frac{1}{2} \|X - B\|_F^2 + \tau \|B\|_* \right\}. \quad (2)$$

The solution to this problem can be explicitly given using the SVDs of $X = U\Sigma V^T$ by $\hat{B} = U\mathbf{S}_\tau(\Sigma)V^T$, where $\mathbf{S}_\tau(\cdot)$ is the element-wise application of the soft-thresholding operator defined as $\mathbf{S}_\tau(x) = \text{sign}(x)(|x| - \tau)_+$. Cai et al. (2010) referred this as the *singular value thresholding* (SVT) method.

It is a well-known fact that the solution to the classical PCA problem is numerically sensitive to the presence of outliers in the data matrix (Lin et al., 2010; Wright et al., 2009; Candès et al., 2011). In other words, if the matrix X is perturbed by one large value, the explicit formula for its low rank approximation would yield a much different solution than the un-perturbed one. On the other hand, ℓ_1 norm does encourage sparsity when the norm is made small. To solve the problem of separating the sparse outliers added to a low-rank matrix, Candès et al. (2011) replaced the Frobenius norm in the SVT problem by the ℓ_1 norm and introduced the *Robust PCA* (RPCA) method (see also Lin et al. (2010)):

$$\min_B \{ \|X - B\|_{\ell_1} + \lambda \|B\|_* \}. \quad (3)$$

Unlike in the classical PCA and SVT problems, the RPCA problem has no closed form solution. Various numerical procedures have been proposed to solve it. Lin et al. (2010), proposed two iterative methods: exact and inexact Augmented Lagrange Method (EALM and iEALM). The iEALM method turns out to be equivalent to the alternating direction method (ADM) later proposed by Tao and Yuan (2011). Wright et al. (2009) proposed the accelerated proximal gradient (APG) method to solve the RPCA problems numerically as well. Note that in all the numerical procedures for solving RPCA, the solution to the SVT problem is used as an important auxiliary step.

In this paper, we propose an alternative solution to the sensitivity of PCAs to the outliers by simply introducing a weight matrix in the Frobenius norm in (2). In particular, using a non-singular weight matrix $W \in \mathbb{R}^{n \times n}$, we focus on the following weighted singular value thresholding (WSVT) problem:

$$\min_B \left\{ \frac{1}{2} \|(X - B)W\|_F^2 + \tau \|B\|_* \right\}, \quad (4)$$

where the weight matrix W is user provided or automatically inferred from the data. Our experiments suggest, a properly inferred weight matrix W may eliminate the effect of the outliers in the data X , sharing the similar spirit as the ℓ_1 norm employed in RPCA. We develop a numerical algorithm to solve WSVT, present the analysis about its convergence, and also conduct some experiments to compare it with RPCA.

We note that using weighted Frobenius norm is not new in low rank matrix approximation problems. In 2003, Srebro and Jaakkola (2003), studied the following weighted low-rank approximation problem: for a given matrix $X \in \mathbb{R}^{m \times n}$ and $r \leq \min\{m, n\}$ find

$$\min_{\substack{B \in \mathbb{R}^{m \times n} \\ r(B) \leq r}} \|(X - B) \odot \tilde{W}\|_F^2, \quad (5)$$

where $\tilde{W} \in \mathbb{R}^{m \times n}$ is a non-negative weight matrix and \odot denotes the element-wise matrix multiplication. They pointed out that, in general, there is no closed form solution to (5). At about the same time, Manton et al. (2003) proposed a problem with a generalized norm:

$$\min_{\substack{B \in \mathbb{R}^{m \times n} \\ r(B) \leq r}} \|X - B\|_Q^2, \quad (6)$$

where $Q \in \mathbb{R}^{mn \times mn}$ is a symmetric positive definite weight matrix, $\|X - B\|_Q^2 := \text{vec}(X - B)^T Q \text{vec}(X - B)$, and $\text{vec}(\cdot)$ is an operator which maps the entries of $\mathbb{R}^{m \times n}$ to vectors in $\mathbb{R}^{mn \times 1}$ by stacking the columns.

The weighted Frobenius norm used in part of the WSVT problem (4) is a special case of both (5) and (6). Note that both (5) and (6) are constrained problems while (4) is an unconstrained problem. Due to the special structure of the WSVT problem, the numerical procedures for solving (5) and (6) proposed in the literature (Srebro and Jaakkola, 2003; Okatani and Deguchi, 2007; Wiberg, 1976; Srebro et al., 2005; Buchanan and Fitzgibbon, 2005; Eriksson and v. d. Hengel, 2012; Markovsky et al., 2006; Markovsky, 2012; Usevich and Markovsky, 2014a,b) cannot be directly applied to solving it. Moreover, we believe WSVT is worth studying as a standalone problem for the following reasons. One is that it serves as a natural alternative to RPCAs in many applications and is computationally inexpensive. The other is that the special structure of the objective function in (4) allows us to present a detailed convergence analysis of the numerical algorithm which is usually hard to obtain in the algorithms for solving (5) and (6) (Srebro and Jaakkola, 2003; Manton et al., 2003; Markovsky et al., 2006; Wiberg, 1976; Okatani and Deguchi, 2007).

To this end, one of our contributions in this paper is a numerical algorithm to solve WSVT with theoretical convergence analysis. An extended study of (4), when the nuclear norm is replaced by $r(B)$ and the regular matrix multiplication with the weight matrix is replaced by more general pointwise multiplication, can be found in Dutta and Li (2017).

The low rank approximation technique has been used to background estimation from the video sequences. In 1999, Oliver et al. (1999) proposed that if the camera motion is presumably static then the background image sequence can be modeled as a low-dimensional linear subspace. Therefore, the foreground layer which is relatively sparse comparing to the slowly changing background layer can be modeled as a sparse ‘‘outlier’’ component of the video sequence. In short, if each frame of the sequence is vectorized and arranged as columns of X , then B , the low-rank matrix is assumed to capture the background information considering $X - B$ sufficiently sparse. In the past decade, a key application of RPCA problems is in background estimation from video sequences. Thus a solution to (3) would give a reasonable estimation of the background frames from a video sequence. On the other hand, the SVT in (2) fails to provide a comparable background estimation (see also Section 4 for some numerical results). We use this experimental setup to test our algorithm

as well as the algorithms for RPCA. For a thorough review of the most recent and traditional algorithms for solving background estimation problem, we refer the reader to Bouwmans (2014), Sobral and Vacavant (2014), and Bouwmans et al. (2016).

The organization of the rest of the paper is as follows. In Section 2, we propose a numerical solution to our WSVT problem for a general non-singular weight matrix W . In Section 3, we present a detailed convergence analysis of our proposed numerical algorithm. In Section 4, using WSVT we propose a robust background estimation model and compare its performance with the RPCA algorithms.

2. Solving the WSVT problem

We propose a numerical algorithm to solve the WSVT problem (4) when W is non-singular. The novelty of our WSVT algorithm is that by using auxiliary variables, we can employ the simple and fast alternating direction method (ADM). Since W is non-singular, we rewrite (4) as:

$$\min_C \left\{ \frac{1}{2} \|XW - C\|_F^2 + \tau \|CW^{-1}\|_* \right\}.$$

Introduce a new variable D with equality constraints as follows: $D = CW^{-1}$. Then above problem becomes

$$\min_{\substack{C, D \\ D=CW^{-1}}} \left\{ \frac{1}{2} \|XW - C\|_F^2 + \tau \|D\|_* \right\}. \quad (7)$$

Next, we use the augmented Lagrange multiplier (ALM) method (Lin et al., 2010; Boyd et al., 2011) to solve this minimization problem. Let

$$L(C, D, Y, \mu) = \frac{1}{2} \|XW - C\|_F^2 + \tau \|D\|_* + \langle Y, D - CW^{-1} \rangle + \frac{\mu}{2} \|D - CW^{-1}\|_F^2$$

be the augmented Lagrangian function where $Y \in R^{m \times n}$ is the Lagrange multiplier and $\mu > 0$, a balancing parameter. To find a numerical solution to the minimization problem $\min_{C, D} L(C, D, Y, \mu)$, we use the alternating direction method via the following iterative updating scheme:

$$\begin{aligned} C_{k+1} &= \arg \min_C L(C, D_k, Y_k, \mu_k), \\ D_{k+1} &= \arg \min_D L(C_{k+1}, D, Y_k, \mu_k). \end{aligned}$$

Note that, by completing the squares and keeping only the relevant terms in the augmented Lagrangian, we have

$$\begin{aligned} \arg \min_C L(C, D_k, Y_k, \mu_k) &= \arg \min_C \left\{ \frac{1}{2} \|XW - C\|_F^2 + \frac{\mu_k}{2} \|D_k - CW^{-1} + \frac{1}{\mu_k} Y_k\|_F^2 \right\}, \\ \arg \min_D L(C_{k+1}, D, Y_k, \mu_k) &= \arg \min_D \left\{ \tau \|D\|_* + \frac{\mu_k}{2} \|D - C_{k+1}W^{-1} + \frac{1}{\mu_k} Y_k\|_F^2 \right\}. \end{aligned}$$

The solution to the first-subproblem can be derived by setting the gradient with respect to C to 0:

$$C_{k+1} = (XW + \mu_k D_k (W^{-1})^T + Y_k (W^{-1})^T) (I + \mu_k (W^T W)^{-1})^{-1};$$

and, the second-subproblem is a SVT problem (2) with $B = C_{k+1} W^{-1} - \frac{1}{\mu_k} Y_k$ and so its solution is

$$D_{k+1} = U_k S_{\tau/\mu_k}(\Sigma_k) V_k^T,$$

where $U_k \Sigma_k V_k^T$ is a SVD of $(C_{k+1} W^{-1} - \frac{1}{\mu_k} Y_k)$. We update Y_k and μ_k by

$$Y_{k+1} = Y_k + \mu_k (D_{k+1} - C_{k+1} W^{-1}); \quad \mu_{k+1} = \rho \mu_k,$$

for a fixed $\rho > 1$. Algorithm 1 presents the full numerical procedure.

Algorithm 1: WSVT algorithm

1 Input : Data matrix $X \in \mathbb{R}^{m \times n}$, weight matrix $W \in \mathbb{R}_+^{n \times n}$ and $\tau > 0, \rho > 1$;
2 Initialize: $C = XW, D = X, Y = 0, \mu > 0$;
3 while *not converged* **do**
4 $C = (XW + \mu D (W^T)^{-1} + Y (W^{-1})^T) (I_n + \mu (W^T W)^{-1})^{-1}$;
5 $[U \ \Sigma \ V] = \text{SVD}(C W^{-1} - \frac{1}{\mu} Y)$;
6 $D = U S_{\frac{\tau}{\mu}}(\Sigma) V^T$;
7 $Y = Y + \mu (D - C W^{-1})$;
8 $\mu = \rho \mu$;
end
9 Output : $B = C W^{-1}$

3. Convergence analysis

In this section we establish the convergence of our algorithm by following the main ideas of Lin et al. (2010) and Oreifej et al. (2013). Recall that $Y_{k+1} = Y_k + \mu_k (D_{k+1} - C_{k+1} W^{-1})$ and define $\hat{Y}_{k+1} := Y_k + \mu_k (D_k - C_{k+1} W^{-1})$. We first state our main results.

Theorem 1 *With the notations introduced above, the following hold.*

(i) *The sequences $\{C_k\}$ and $\{D_k\}$ are convergent. Moreover,*

$$\|D_k - C_k W^{-1}\| \leq \frac{C}{\mu_k}, \quad k = 1, 2, \dots,$$

for some constant C independent of k .

(ii) *If $L_{k+1} := L(C_{k+1}, D_{k+1}, Y_k, \mu_k)$, then the sequence $\{L_k\}$ is bounded above and*

$$L_{k+1} - L_k \leq \frac{\mu_k + \mu_{k-1}}{2} \|D_k - C_k W^{-1}\|_F^2 = O\left(\frac{1}{\mu_k}\right), \quad \text{for } k = 1, 2, \dots.$$

Theorem 2 Let (C_∞, D_∞) be the limit point of (C_k, D_k) and define

$$f_\infty = \frac{1}{2} \|XW - C_\infty\|_F^2 + \tau \|D_\infty\|_*.$$

Then $C_\infty = D_\infty W$ and

$$-O(\mu_{k-1}^{-2}) \leq \frac{1}{2} \|XW - C_k\|_F^2 + \tau \|D_k\|_* - f_\infty \leq O(\mu_{k-1}^{-1}).$$

We provide the proofs of Theorems 1 and 2 in Appendix A.

4. Experimental results

In this section, as a proof of concept, we demonstrate the performance of our WSVT algorithm on two computer vision applications: background estimation from video sequences and shadow removal from face images under varying illumination conditions. We show that, with a diagonal weight matrix W , we can improve the performance or achieve similar results as compared with other state-of-the-art unweighted low-rank algorithms, especially RPCAs.

4.1 Background estimation

Background estimation from video sequences is a classic computer vision problem. One can consider the scene in the background is presumably static; thus, the background component is expected to be the low-rank part of the matrix X that concatenates the video frames. Minimizing the rank of the matrix X emphasizes the structure of the linear subspace containing the column space of the background. However, the exact desired rank is often tuned empirically, as the ideal rank-one background is often unrealistic.

In our experiments, we use three different sequences: (i) the Stuttgart synthetic video data set (Brutzer et al., 2011), (ii) the airport hall sequence, and (iii) the fountain sequence from the PTIS dataset (Li et al., 2004). We give qualitative analysis results on all three sequences. For performing the quantitative analysis between different methods, we use the Stuttgart video sequence. It is a computer generated sequence from the vantage point of a static camera located on the side of a building viewing a city intersection. The reason for choosing this sequence is two-fold. First, this is a challenging video sequence which comprises both static and dynamic foreground objects and varying illumination in the background. Second, because of the availability of ample amount of ground truth, we can provide a rigorous quantitative comparison of the various methods. We choose the first 600 frames of the *Basic* scenario to capture the changing illumination and foreground object. Correspondingly, we have 600 ground truth frames. The frames and ground truths are resized to 64×80 and each is vectorized to a column vector of size 5120×1 . Denote by the matrix as the concatenation of all the video frames, $X = \{vec(I_1), vec(I_2), \dots, vec(I_{600})\}$, where $vec(I_i) \in \mathbb{R}^{5120 \times 1}$ and $I_i \in \mathbb{R}^{64 \times 80}$. Figure 1 shows a sample video frame of the *Basic* scenario and the corresponding ground truth mask from the Stuttgart video sequence and demonstrates an outline of processing the video frames defined above.

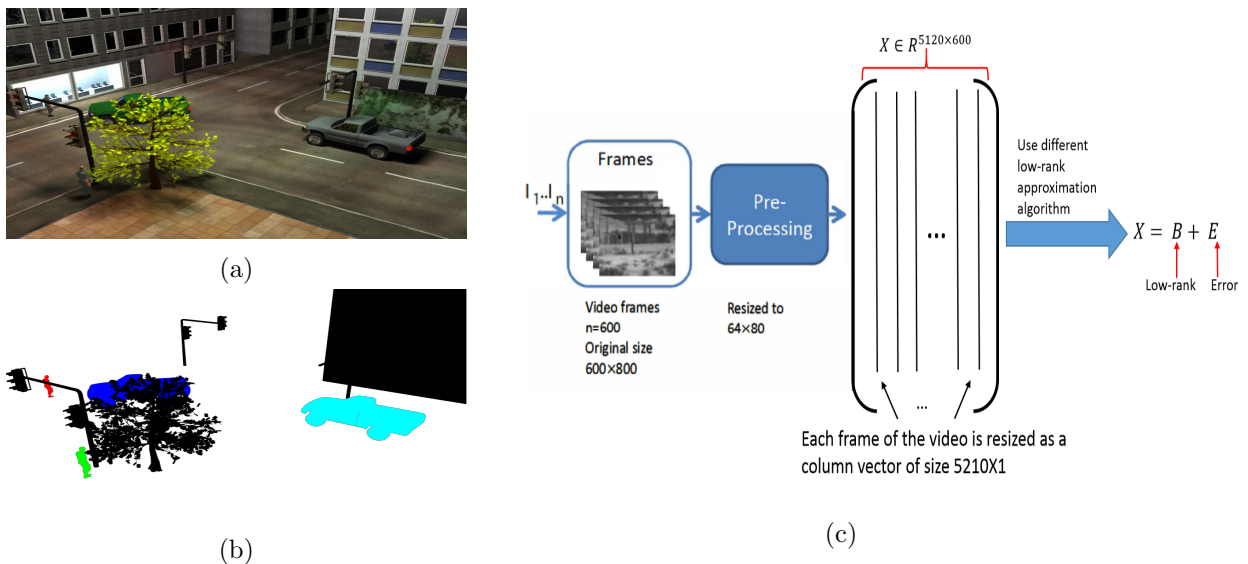


Figure 1: (a) Sample frame from the Stuttgart artificial video sequence and (b) the corresponding ground truth mask. (c) The framework for background estimation.

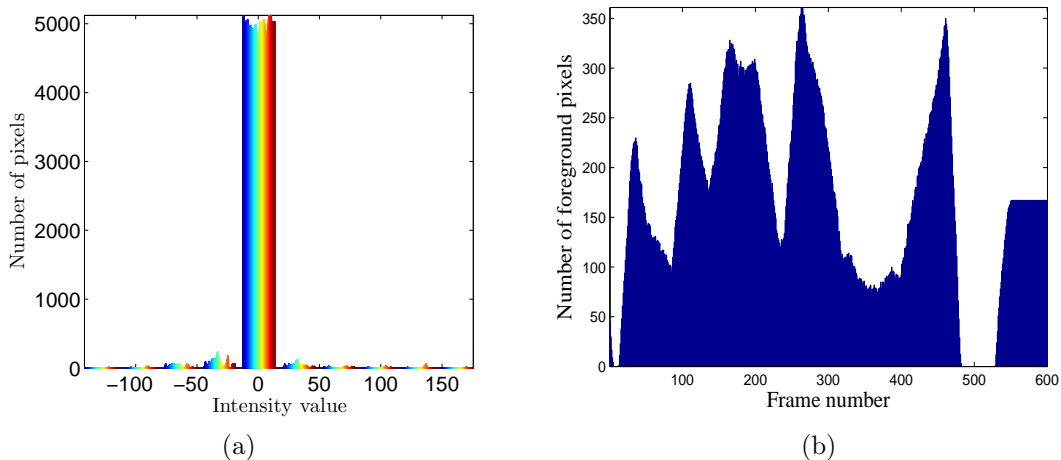


Figure 2: Stuttgart video sequence *Basic* scenario: (a) Histogram to choose the threshold $\epsilon_1 = 31.2202$. (b) Sums of the logical values within each ground truth frame, where the frames with zero foreground pixels are purely background frames. See text for more details.

We compare the performance of our algorithm to RPCA and SVT methods. We set a uniform threshold 10^{-7} for each method. For iEALM and APG, the two prevalent algorithms for RPCA, we set $\lambda = 1/\sqrt{\max\{m, n\}}$, and for iEALM we choose $\mu = 1.5, \rho = 1.25$ (Wright et al., 2009; Candès et al., 2011; Lin et al., 2010). To choose the right set of parameters for WSVT, we perform a grid search using a small holdout subset of frames. For WSVT, we set $\tau = 4500, \mu = 5, \rho = 1.1$ for a fixed weight matrix W . For SVT, we set $\tilde{\tau} = \tau/\mu$ since

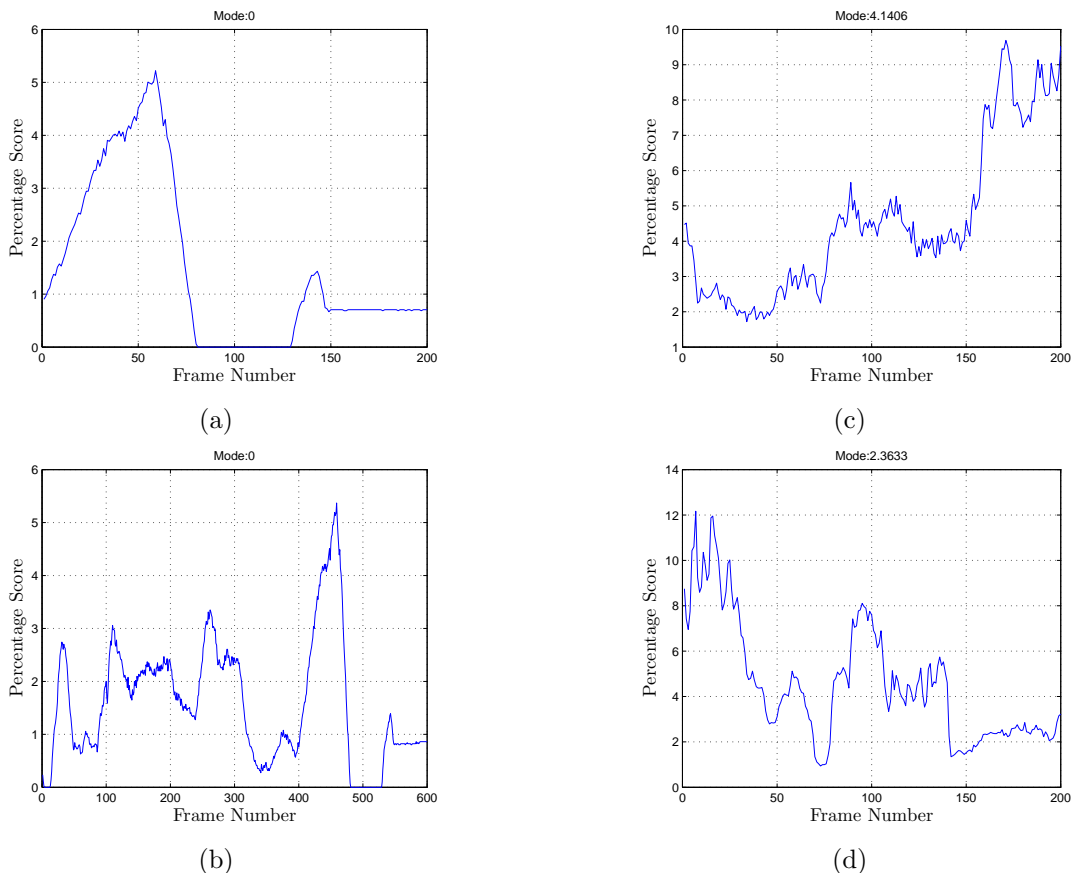


Figure 3: **Robust weight learning.** Frame number versus Percentage score for Stuttgart video sequence *Basic* scenario: (a) on last 200 frames, and (b) on the entire sequence. Originally, there are 46 frames and 53 frames in the last 200 frames and the entire sequence respectively, with no foreground. We also show the percentage scores versus frame numbers on the first 200 frames for: (c) the fountain sequence, and (b) the airport hall sequence.

our method is equivalent to SVT for $W = I_n$. Next, we show the effectiveness of our WSVT and a mechanism for automatically estimating the weights from the data.

4.1.1 ESTIMATING THE WEIGHT MATRIX W IN OUR WSVT

We present a mechanism for estimating the weights from the data for WSVT. We use the heuristic that the data matrix X can be comprised of two blocks X_1 and X_2 such that X_1 mainly contains the information about the background frames which have the least foreground movements.

Therefore, we want to choose a large weight $\tilde{\lambda}$ corresponding to the frames of X_1 . However, the changing illumination, reflection, and noise are typically also a part of those frames and pose a lot of challenges. We thus instead recover a low-rank matrix $B = (B_1 \ B_2)$ with compatible block partition such that $B_1 \approx X_1$. For this purpose, the main idea is to have a coarse estimation of the background using an identity weight matrix, infer the weights

from the coarse estimation, and then use the inferred weights to refine the background. We denote the test matrix as T , and ground truth matrix as G . We borrow some notations from MATLAB to explain the experimental setup. Note that, the last 200 frames of the Stuttgart video sequence are the most challenging among the sequence, containing static foreground (last 50 frames) along with moving foreground object and varying illumination.

We use our method with $W = I_n$ for 2 iterations on the frames, and then detect the initial foreground F_{I_n} and background B_{I_n} . It might not be the best practice to specify the number of foreground/background pixels manually for each test video sequence. Instead, we propose an automatic mechanism. We plot the histogram of our initially detected foreground to determine the threshold ϵ_1 of the intensity value. In our experiments on the Stuttgart video sequence *Basic* scenario, we pick $\epsilon_1 = 31.2202$, the second smallest value of $|(F_{I_n})_{ij}|$, where $|\cdot|$ denotes the absolute value (see Figure 2).

We replace everything below ϵ_1 by 0 in F_{I_n} , and convert it into a logical matrix LF_{I_n} . Arguably, for each such logical video frame, the number of pixels whose values are on (+1) is a good indicator about whether the frame is mainly about the background. Note that $\sum_{i=1}^m (LF_{I_n})_{ij}$ is the j th column sum of LF_{I_n} . We convert B_{I_n} directly to a logical matrix LB_{I_n} and define percentage score as the ratio of total foreground and background pixels converted into percentage. We calculate the percentage score of each video frame and choose the threshold ϵ_2 as

$$\epsilon_2 := \text{mode}(\{ \frac{\sum_i (LF_{I_n})_{i1}}{\sum_i (LB_{I_n})_{i1}} \times 100, \frac{\sum_i (LF_{I_n})_{i2}}{\sum_i (LB_{I_n})_{i2}} \times 100, \dots, \frac{\sum_i (LF_{I_n})_{in}}{\sum_i (LB_{I_n})_{in}} \times 100 \}),$$

where $\{ \frac{\sum_i (LF_{I_n})_{ij}}{\sum_i (LB_{I_n})_{ij}} \times 100 \}_{j=1}^n$ are the percentage score of each frame. Since the foreground pixels are relatively smaller size compared to the background, heuristically the possible contender of the pure background frame indexes will have percentage score less than ϵ_2 . Therefore, the frame indexes with least foreground movement are chosen from the following set:

$$I = \{i : (\frac{\sum_i (LF_{I_n})_{i1}}{\sum_i (LB_{I_n})_{i1}} \times 100, \frac{\sum_i (LF_{I_n})_{i2}}{\sum_i (LB_{I_n})_{i2}} \times 100, \dots, \frac{\sum_i (LF_{I_n})_{in}}{\sum_i (LB_{I_n})_{in}} \times 100) \leq \epsilon_2\}.$$

Figure 2 shows the initially estimated foreground histogram and the sums of the ground truth frames of the *Basic* scenario of the Stuttgart video sequence. Figure 3 demonstrates the percentage score plot for the *Basic* scenario of the Stuttgart video sequence, the fountain sequence, and the airport hall sequence. Originally, for the *Basic* scenario of the Stuttgart video sequence, there are 48 and 57 frames respectively in the last 200 frames and the entire sequence that have less than 5 foreground pixels. Using the percentage score, our method picks up 49 and 58 frame indexes respectively. Moreover, comparing Figure 3(a) and (b) with the ground truth frames in Figures 2 (b), we see the effectiveness of the process in picking up the right background frame indexes on the Stuttgart video sequence.

With the automatically inferred diagonal weight matrix W , whose entries corresponding to the coarsely estimated background information are assigned a large value $\tilde{\lambda}$ and other diagonal entries are 1's, we conduct the remaining experiments.

4.1.2 CONVERGENCE OF THE ALGORITHM

In this subsection, we will show the convergence of our WSVT algorithm. For a given $\epsilon > 0$, the main stopping criteria of our WSVT algorithm is $|L_{k+1} - L_k| < \epsilon$ or if it reaches the

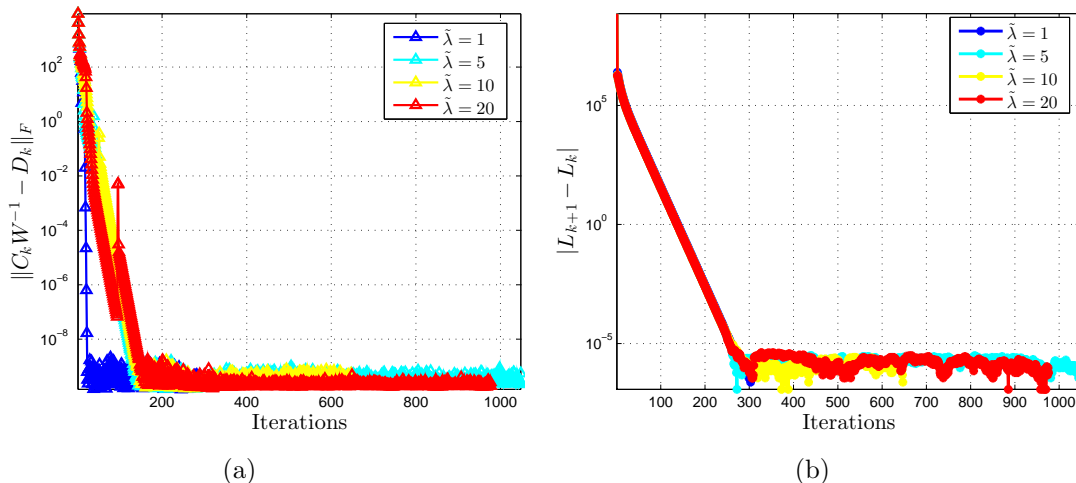


Figure 4: **Convergence of the algorithm.** For $\tilde{\lambda} \in \{1, 5, 10, 20\}$: (a) Iterations versus $\|D_k - C_k W^{-1}\|_F$, and (b) Iterations versus $|L_{k+1} - L_k|$.

maximum iteration. To demonstrate the convergence of our algorithm as claimed in Theorem 1, we run it on the *Basic* scenario of the Stuttgart artificial video sequence. The weights were chosen using the idea explained in Subsection 4.1.1. We choose $\tilde{\lambda} \in \{1, 5, 10, 20\}$ and ϵ is set to 10^{-7} . Recall that in Theorem 1 we present $\|D_k - C_k W^{-1}\| \leq O(\frac{1}{\mu_k})$ and $|L_{k+1} - L_k| \leq O(\frac{1}{\mu_k})$ as $\mu_k \rightarrow \infty$. We see that our proposed algorithm converges and the bounds we present on the iterates $\{C_k, D_k\}$ and the reconstruction error L_k in Theorem 1 are valid. To conclude, in Figure 4, we show that for any $\tilde{\lambda} > 0$, there exists $\alpha, \beta \in \mathbb{R}$ such that $\|D_k - C_k W^{-1}\|_F \leq \alpha/\mu_k$ and $|L_{k+1} - L_k| \leq \beta/\mu_k$ as $\mu_k \rightarrow \infty$, for $k = 1, 2, \dots$.

4.1.3 QUALITATIVE AND QUANTITATIVE ANALYSIS

In this section, we perform rigorous qualitative and quantitative comparison between WSVT, SVT, and RPCA algorithms on three different video sequences: Stuttgart artificial video sequence, the airport hall sequence, and the fountain sequence. For the quantitative comparison between different methods, we only use Stuttgart artificial video sequence. We use three different metrics for quantitative comparison: The receiver and operating characteristic (ROC) curve, peak signal-to-noise ratio (PSNR) and the mean structural similarity index (MSSIM) (Wang et al., 2004). They are all methods for measuring the similarity between two images – in our scenario, the ground truth and estimated foreground.

Initially, we test each method on 200 resized video frames and the qualitative results are shown in Figure 5. We employ the process defined in Section 4.1.1 to adaptively choose the weighted frame indexes for WSVT. Next, we test our method on the entire Stuttgart video sequence and compare its performance with the other unweighted low-rank methods. Unless specified, a weight $\tilde{\lambda} = 5$ is used to show the qualitative results for the WSVT algorithm in Figure 5 and 6. It is evident from Figure 5 that WSVT outperforms SVT and recovers the background as effectively as RPCA methods. However, in Figure 6 where there are both

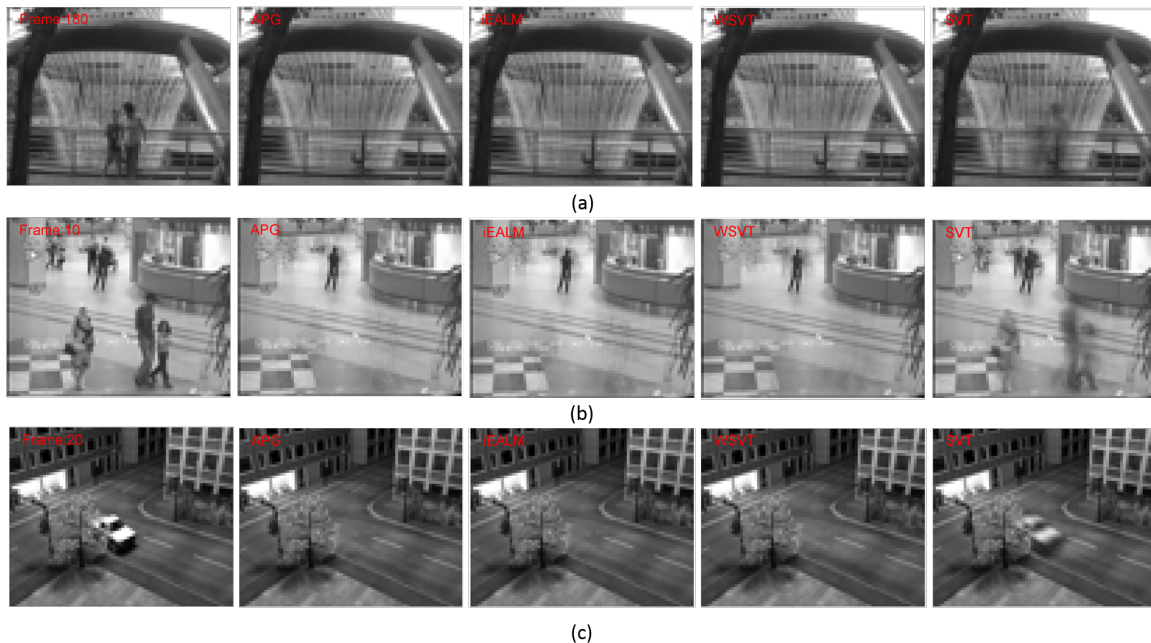


Figure 5: **Qualitative analysis:** From left to right: Original, APG, iEALM, our WSVT, and SVT. Background estimation results on (from top to bottom): (a) fountain sequence, frame number 180 with static and dynamic foreground; (b) airport sequence, frame number 10 with static and dynamic foreground; (c) Stuttgart video sequence *Basic* scenario, frame number 420 with dynamic foreground.

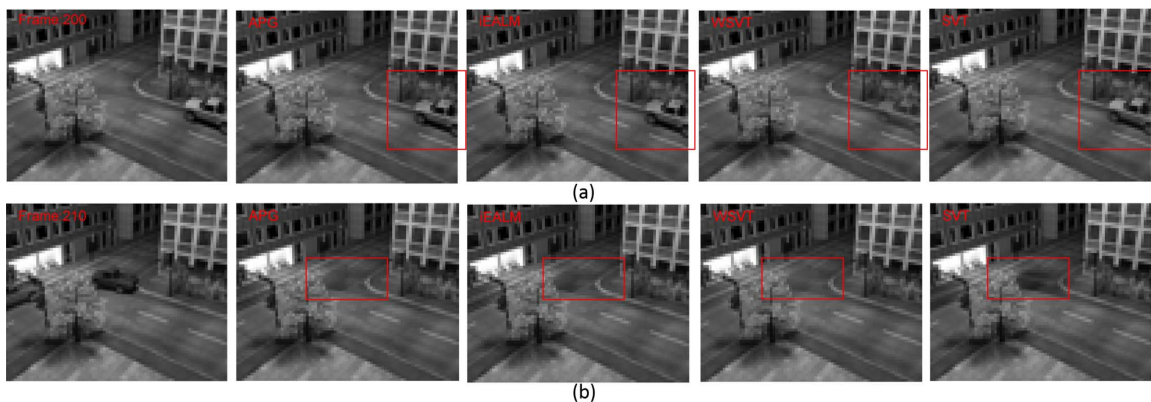


Figure 6: **Qualitative analysis:** From left to right: Original, APG, iEALM, WSVT, and SVT on Stuttgart video sequence *Basic* scenario: (a) frame 600 with static foreground, methods were tested on last 200 frames; (b) frame 210 with dynamic foreground, methods were tested on 600 frames. WSVT provides a superior background estimation.

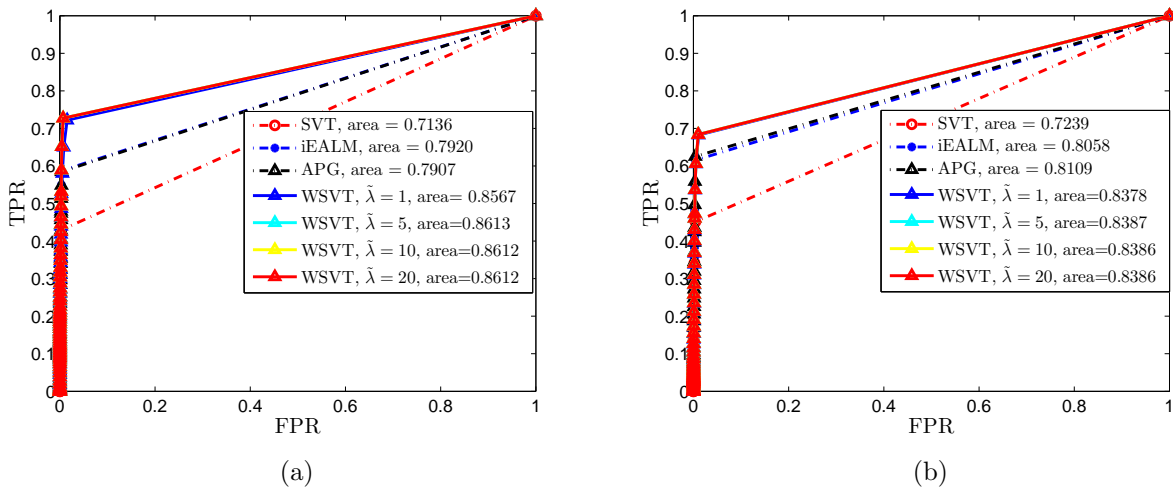


Figure 7: ROC curve for the methods WSVT, SVT, iEALM, and APG on *Basic* scenario of the Stuttgart sequence:(a) 200 frames, and (b) 600 frames. For WSVT we choose $\tilde{\lambda} \in \{1, 5, 10, 20\}$. The performance gain by WSVT compare to iEALM, APG, and SVT are: 8.92%, 8.74%, and 20.68% respectively on 200 frames (with static foreground), and 4.07%, 3.42%, and 15.85% respectively on 600 frames.

static and dynamic foreground objects, WSVT shows superior performance over all other methods including RPCA algorithms.

Quantitative analysis. Note that WSVT uniformly removes the noise (for example, the changing illumination, reflection on the buildings, and movement of the leaves of the tree for the Stuttgart sequence) from each video sequence. Inspired by the above observation, we propose a nonuniform threshold vector to plot the ROC curves and compare between the methods using the same metric. In Figure 7, we provide quantitative comparisons between the methods using this non-uniform threshold vector $[0, 15, 20, 25, 30, 31 : 2.5 : 255]$. This way we can reduce the number of false negatives and increase the number of true positives detected by WSVT as it appears in Figure 5, 6 . To conclude, WSVT has better quantitative and qualitative results when there is a static foreground in the video sequence.

A robust background estimation model used for surveillance may efficiently deal with the dynamic foreground objects present in the video sequence. Additionally, it is expected to handle several other challenges, which include, but are not limited to: gradual or sudden change of illumination, a dynamic background containing non-stationary objects and a static foreground, camouflage, and sensor noise or compression artifacts. The initial success of the WSVT in Figure 7 on the *Basic* scenario of the Stuttgart sequence motivated us to demonstrate a more rigorous quantitative measure of the recovered foreground obtained by different background estimation models on a more challenging scenario. For this purpose, we test the effectiveness of the models on the *Noisy night* scenario of the Stuttgart video sequence. This is a low-contrast nighttime scene, with increased sensor noise, camouflage, and sudden illumination change and has 600 frames with identical foreground and background objects as in the *Basic* scenario. Now, we demonstrate the quantitative analysis results of

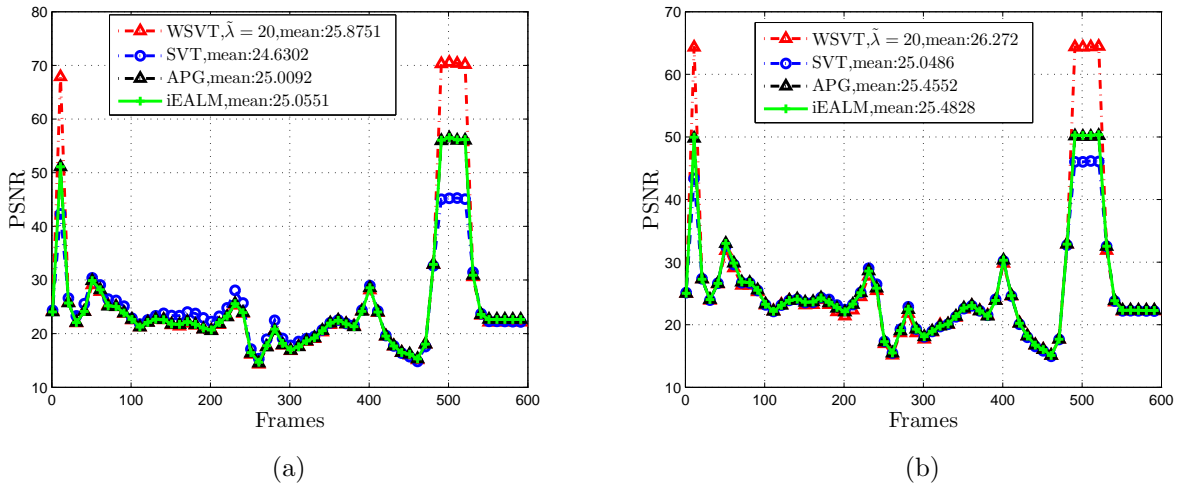


Figure 8: PSNR of each video frame for WSVT, SVT, iEALM, and APG on:(a) *Basic* scenario, and (b) *Noisy night* scenario. For WSVT we choose $\tilde{\lambda} = 20$. In both scenarios WSVT has increased PSNR when a weight is introduced corresponding to the frames with least foreground movement.

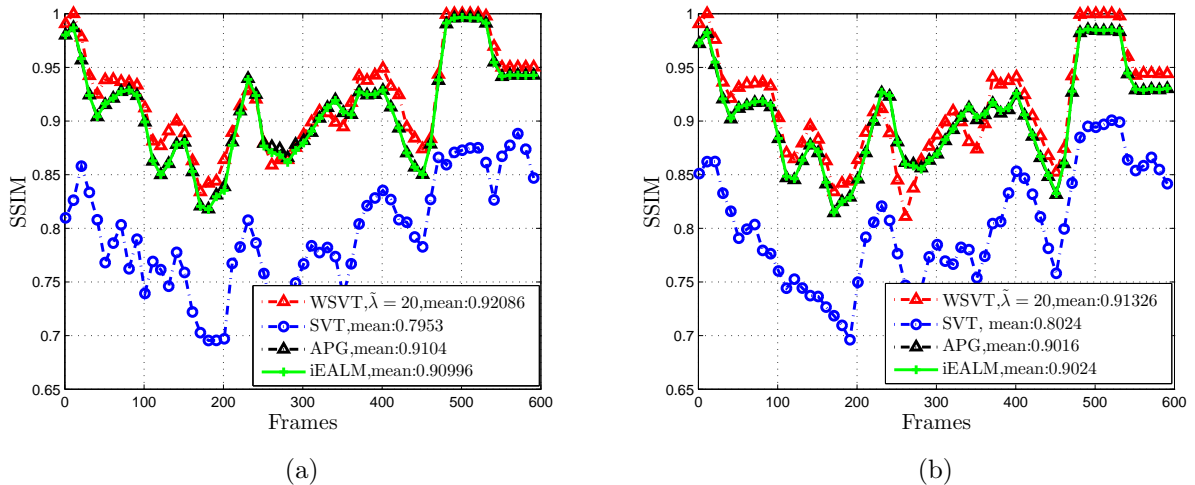


Figure 9: Mean SSIM for different methods on 600 frames of Stuttgart sequence: (a) *Basic* scenario, (b) *Noisy night* scenario. For WSVT we choose $\tilde{\lambda} = 20$. Indeed WSVT with weight outperforms other methods.

different methods on these two scenarios using PSNR and SSIM. We use the same set of parameters for every model and follow Section 4.1.1 to choose weighted frames for WSVT.

PSNR is defined as $10 \log_{10}$ of the ratio of the peak signal energy to the mean square error (MSE) observed between the processed video signal and the original video signal. If $E(:, i)$ denotes each reconstructed vectorized foreground frame in the video sequence and $G(:, i)$ be the corresponding ground truth frame, then PSNR is defined as $10 \log_{10} \frac{M^2}{\text{MSE}}$, where

$MSE = \frac{1}{mn} \|E(:, i) - G(:, i)\|_2^2$ and M_I is the maximum possible pixel value of the image. In our case the pixels are represented using 8 bits per sample, and therefore, M_I is 255. The proposal is that the higher the PSNR, the better degraded image has been reconstructed to match the original image and the better the reconstructive algorithm. This would occur because we wish to minimize the MSE between images with respect the maximum signal value of the image. For a reconstructed image with 8 bits bit depth, the PSNR are between 30 and 50 dB, where the higher is the better.

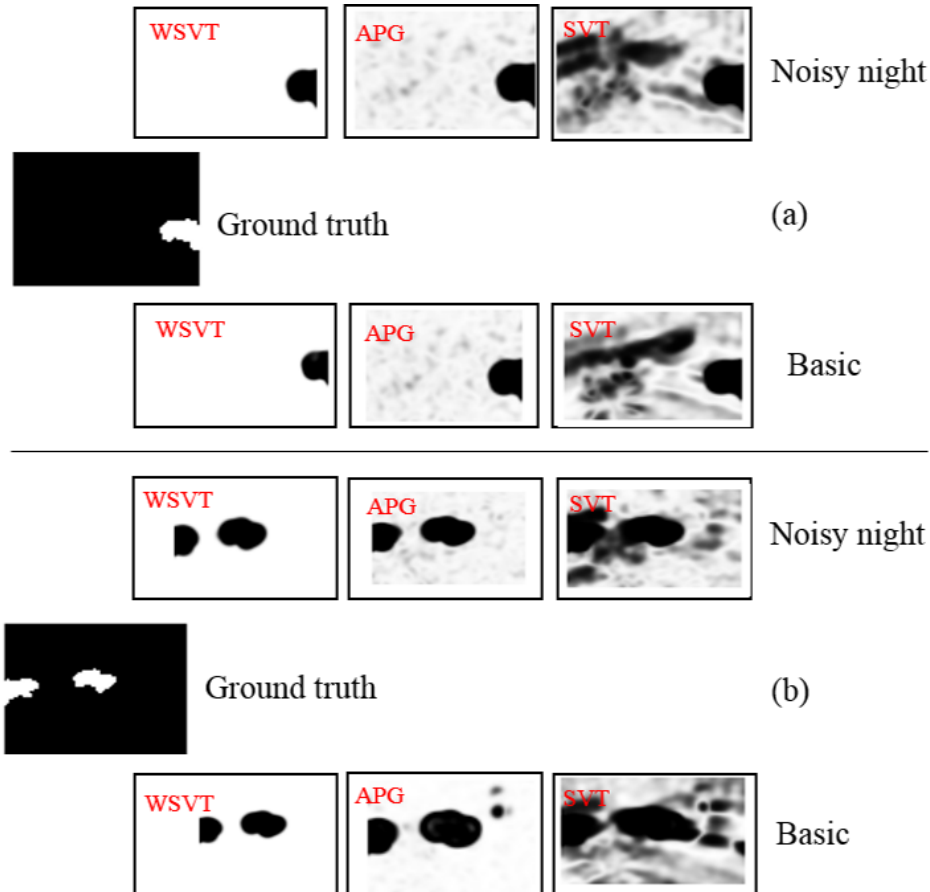


Figure 10: SSIM map of foreground frame: (a) 600 and (b) 210. Since iEALM and APG have same recovered foreground we only provide SSIM map for APG. Indeed WSVT with $\tilde{\lambda} = 20$ has the best foreground reconstruction. The foreground recovered by SVT is very poor and RPCA recovers fragmentary foreground.

In Figure 8, we demonstrate the PSNR and mean PSNR of different methods on the Stuttgart sequence on two different scenarios. For their implementation, we calculate the PSNR of the entire video sequence for each scenario and compare with the ground truth frames. It is evident from Figure 8 that weight improves the PSNR of WSVT significantly over the other existing methods in both scenarios of the Stuttgart sequence. More specifically, we see that in both scenarios the weighted background frames or the frames with least foreground movement have higher PSNR than all other models traditionally used for

background estimation. In Figure 8 (a), for $\tilde{\lambda} = 20$ in WSVT, PSNR of the frames with least foreground movement is above 65 dB. Similarly, in Figure 8 (b), for the *Noisy night* scenario, the PSNR of the frames with least foreground movement is about 65 dB when $\tilde{\lambda} = 20$.

Recently, the structural similarity index (SSIM) is considered to be one of the most robust quantitative measures and claimed to agree with the human visual perception better compare to the widely used standard measures, such as, MSE and PSNR (Wang et al., 2004). In calculating the MSSIM, we perceive the information how the high-intensity regions of the image are coming through the noise, and consequently, we pay much less attention to the low-intensity regions. We remove the noisy components from the recovered foreground, E , by using the threshold ϵ_1 calculated in Section 4.1.1, such that we set the components below ϵ_1 in E to 0. In order to calculate the MSSIM of each recovered foreground video frame, we consider an 11×11 Gaussian window with standard deviation (σ) 1.5 and consider the corresponding ground truth as the reference image.

The SSIM index of WSVT in Figure 9 shows the superior performance of WSVT especially in presence of the static foreground in both scenarios. Additionally, from Figure 9 we observe the comparable or superior performance of WSVT on rest of the frames of both scenarios, except a minor deterioration in some frames of the *Noisy night* scenario. Moreover, the superior performance of WSVT over other models in Figure 8 and 9 show the validity of the method proposed in Section 4.1.1 in choosing the correct weighted frame indexes. In Figure 10, we present SSIM index map of two sample foreground video frames of Stuttgart video sequence from both scenarios, which clearly indicate fragmentary foreground recovered by the RPCA algorithms.

4.2 Facial Shadow Removal

We also conduct some experiments on the removal of shadow and specularities from face images under varying illuminations and camera positions. The idea was proposed by Basri and Jacobs (2003), that the images of the same face exposed to a wide variety of lighting conditions can be approximated accurately by a low-dimensional linear subspace. More specifically, the images under distant, isotropic lighting lie close to a 9-dimensional linear subspace which is known as the *harmonic plane*.



Figure 11: **Qualitative results for facial shadow removal.** Left to right: Original image (person B11, image 56, partially shadowed) followed by the low-rank approximations using APG, SVT, and WSVT, respectively. WSVT removes the shadows and specularities uniformly from the face image especially from the left half of the image.

For facial shadow removal we use test images from the Extended Yale Face Database B ((Georghiades et al., 2001); see also, <http://vision.ucsd.edu/content/extended-yale-face-database-b-b>). We choose 65 sample images and perform our experiments. The images are resized to [96,128]; originally they are [480,640]. We set a uniform threshold 10^{-7} for each algorithm. For APG and iEALM, $\lambda = 1/\sqrt{\max\{m,n\}}$, and the parameters for iEALM are set to $\mu = 1.5, \rho = 1.25$ (Wright et al., 2009; Lin et al., 2010). For WSVT we choose $\tau = 500, \mu = 15,$ and $\rho = 3$. The weight matrix is set to I_n . For SVT, we choose $\tilde{\tau} = \tau/\mu$. Since we have no access to the ground truth for this experiment we will only provide the qualitative result. Note that the rank of the low-dimensional linear model recovered by RPCA methods is 35, while SVT and WSVT are both able to find a rank 4 subspace. Figure 11 shows that WSVT outperforms RPCA algorithms and SVT in terms of the shadow removal results.

4.3 Computation time comparison

Tables 1 and 2 contrast the computation cost of our WSVT to other methods on both sets of experiments: background estimation and facial shadow removal. It is easy to see that WSVT is more efficient than the RPCA algorithms (iEALM and APG) especially when the video sequence is long. Recall that the performance of WSVT is better than or on par with RPCAs. We thus expect that WSVT can be an efficient and effective alternative to RPCAs in more applications.

Table 1: Average computation time (in seconds) for each algorithm in background estimation on the Stuttgart sequence *Basic* scenario. All experiments were performed on a computer with 3.1 GHz Intel Core i7 processor and 8GB memory.

No. of frames	iEALM	APG	SVT	WSVT
200	4.994787	14.455450	0.085675	1.4468
600	131.758145	76.391438	0.307442	8.7885334

Table 2: Average computation time (in seconds) for each algorithm in shadow removal.

No. of images	iEALM	APG	SVT	WSVT
65	1.601427	10.221226	0.039598	1.047922

5. Conclusion and Future Research

We formulated and studied a weighted version of the SVT method (WSVT) and proposed a numerical algorithm to solve WSVT using augmented Lagrangian function and alternating direction method. We managed to establish the convergence of our algorithm. Through real data, we demonstrated that by using the weight, which can be learned from the data, we can gain better performance than RPCAs in several applications in computer vision. In

particular, our algorithm shows better quantitative results in Stuttgart video sequence and facial shadow removal compare to other state-of-the-art unweighted low-rank algorithms.

Determining the weights adaptively is a challenging and mathematically involved problem and a good starting point for future research. Initially we tuned the parameters for our method using a grid search, but in future the parameters may be trained jointly with the low-rank matrix in a more robust fashion. We also plan on testing the potential applications of our method by exploring research areas like domain adaptation and video summarization.

Appendix A.

In this section, we will provide the proofs of the convergence results stated in Section 3. To establish our main results, we need two lemmas. First, we establish the boundedness of Y_k :

Lemma 3 *The sequence $\{Y_k\}$ is bounded.*

Proof By the optimality condition for D_{k+1} we have,

$$0 \in \partial_D L(C_{k+1}, D_{k+1}, Y_k, \mu_k).$$

So,

$$0 \in \tau \partial \|D_{k+1}\|_* + Y_k + \mu_k(D_{k+1} - C_{k+1}W^{-1}).$$

Therefore, $-Y_{k+1} \in \tau \partial \|D_{k+1}\|_*$. By using Theorem 4 in (Lin et al., 2010), (see also Watson (1992)), we conclude that the sequence $\{Y_k\}$ is bounded by τ in the dual norm of $\|\cdot\|_*$. But the dual of $\|\cdot\|_*$ is the spectral norm, $\|\cdot\|_2$. So $\|Y_{k+1}\|_2 \leq \tau$. Hence $\{Y_k\}$ is bounded. ■

Next, we show the boundedness of the sequence $\{\hat{Y}_k\}$ which requires a different argument.

Lemma 4 *We have the following:*

- (i) *The sequence $\{C_k\}$ is bounded.*
- (ii) *The sequence $\{\hat{Y}_k\}$ is bounded.*

Proof We start with the optimality of C_{k+1} :

$$0 = \frac{\partial}{\partial C} L(C_{k+1}, D_k, Y_k, \mu_k).$$

We get

$$(C_{k+1}W^{-1} - X)WW^T = Y_k + \mu_k(D_k - C_{k+1}W^{-1}). \quad (8)$$

- (i) Solving for D_k in (8), we arrive at

$$D_k = C_{k+1}(W^{-1} + \frac{1}{\mu_k}W^T) - \frac{1}{\mu_k}(XWW^T - Y_k).$$

Next, using the definition of $\{Y_k\}$ to write

$$D_k = C_k W^{-1} - \frac{1}{\mu_{k-1}} Y_{k-1} + \frac{1}{\mu_{k-1}} Y_k$$

and now equating the two expressions for D_k to obtain

$$C_k W^{-1} - \frac{1}{\mu_{k-1}} Y_{k-1} + \frac{1}{\mu_{k-1}} Y_k = C_{k+1} (W^{-1} + \frac{1}{\mu_k} W^T) - \frac{1}{\mu_k} (X W W^T - Y_k).$$

To simplify the notations, we will use $O(\frac{1}{\mu_k})$ to denote matrices whose norm is bounded by a constant (independent of k) times $\frac{1}{\mu_k}$. So, by using the boundedness of $\{Y_k\}$, the above equation can be written as

$$C_{k+1} (I + \frac{1}{\mu_k} W^T W) = C_k + O(\frac{1}{\mu_k}). \quad (9)$$

Diagonalize the positive definite matrix $W^T W$ as $W^T W = Q \Lambda Q^T$ and use it in (9) to get

$$C_{k+1} Q (I + \frac{1}{\mu_k} \Lambda) = C_k Q + O(\frac{1}{\mu_k}).$$

Taking the Frobenius norm on both sides and using the triangle inequality yield

$$\|C_{k+1} Q (I + \frac{1}{\mu_k} \Lambda)\|_F \leq \|C_k Q\|_F + O(\frac{1}{\mu_k}). \quad (10)$$

Since the diagonal matrix $I + \frac{1}{\mu_k} \Lambda$ has all diagonal entries no smaller than $1 + \lambda/\mu_k$ where $\lambda > 0$ denotes the smallest eigenvalue of $W^T W$, we see that

$$\|C_{k+1} Q\|_F \leq (1 + \frac{\lambda}{\mu_k})^{-1} \|C_{k+1} Q (I + \frac{1}{\mu_k} \Lambda)\|_F.$$

Thus, (10) implies

$$\|C_{k+1} Q\|_F \leq (1 + \frac{\lambda}{\mu_k})^{-1} \|C_k Q\|_F + O(\frac{1}{\mu_k}),$$

which, by the unitary invariance of the norm, is equivalent to

$$\|C_{k+1}\|_F \leq (1 + \frac{\lambda}{\mu_k})^{-1} \|C_k\|_F + \frac{C}{\mu_k} \text{ for all } k,$$

for some constant $C > 0$ independent of k . Finally, using the fact that $\mu_{k+1} = \rho \mu_k$ with $\rho > 1$, we see that the above inequality implies (by mathematical induction) that $\|C_k\|_F \leq C^*$ for some constant $C^* > 0$ (say, $C^* = C(\mu_0 + \lambda)/(\mu_0 \lambda)$ would work). This completes the proof of the boundedness of $\{C_k\}$.

- (ii) Equation (8) gives us $\hat{Y}_{k+1} = (C_{k+1} W^{-1} - X) W W^T$ by using the definition of \hat{Y}_{k+1} , and so, the boundedness of $\{\hat{Y}_k\}$ follows immediately from the boundedness of $\{C_k\}$ established in (i) above. ■

With the boundedness results of the sequences $\{Y_k\}$, $\{C_k\}$, and $\{\hat{Y}_k\}$, we are ready to prove Theorems 1 and 2.

Proof of Theorem 1

(i) Since $Y_{k+1} - \hat{Y}_{k+1} = \mu_k(D_{k+1} - D_k)$ we have

$$D_{k+1} - D_k = \frac{1}{\mu_k}(Y_{k+1} - \hat{Y}_{k+1}).$$

So, by the boundedness of $\{Y_k\}$ and $\{\hat{Y}_k\}$ from Lemma 3 and 4, for all k , we have

$$\|D_{k+1} - D_k\| = O\left(\frac{1}{\mu_k}\right),$$

which, by comparison test, implies the convergence of $\{D_k\}$. Now, recall that

$$C_{k+1} = (XW + \mu_k D_k (W^{-1})^T + Y_k (W^{-1})^T)(I + \mu_k (W^T W)^{-1})^{-1}.$$

So, we see that $\{C_k\}$ is convergent as well. Next, from the definition of $\{Y_k\}$, we have

$$\frac{1}{\mu_k}(Y_{k+1} - Y_k) = D_{k+1} - C_{k+1}W^{-1}.$$

Thus,

$$\|D_{k+1} - C_{k+1}W^{-1}\| = O\left(\frac{1}{\mu_k}\right). \quad (11)$$

(ii) We have, $L_{k+1} = L(C_{k+1}, D_{k+1}, Y_k, \mu_k) \leq L(C_{k+1}, D_k, Y_k, \mu_k) \leq L(C_k, D_k, Y_k, \mu_k)$. Note that, $L(C_k, D_k, Y_k, \mu_k) = L_k + \frac{\mu_k + \mu_{k-1}}{2} \|D_k - C_k W^{-1}\|_F^2$. Therefore,

$$L_{k+1} - L_k \leq \frac{\mu_k + \mu_{k-1}}{2} \|D_k - C_k W^{-1}\|_F^2.$$

Since $\mu_{k+1} = \rho\mu_k$, we find, using (11),

$$L_{k+1} - L_k \leq \frac{\mu_k + \mu_{k-1}}{2} \|D_k - C_k W^{-1}\|_F^2 = O\left(\frac{1}{\mu_k}\right), \text{ as } k \rightarrow \infty.$$

This completes our proof of Theorem 1. ■

Proof of Theorem 2 By Theorem 1 (i) and by taking the limit as $k \rightarrow \infty$, we get

$$C_\infty W^{-1} = D_\infty. \quad (12)$$

Note that

$$\begin{aligned} L(C_k, D_k, Y_{k-1}, \mu_{k-1}) &= \min_{C, D} L(C, D, Y_{k-1}, \mu_{k-1}) \\ &\leq \min_{C W^{-1} = D} L(C, D, Y_{k-1}, \mu_{k-1}) \\ &\leq \|XW - C_\infty\|_F^2 + \tau \|D_\infty\|_* \\ &= f_\infty, \end{aligned} \quad (13)$$

where we applied (12) to get the last inequality. Note also that

$$\begin{aligned} & \|XW - C_k\|_F^2 + \tau\|D_k\|_* \\ &= L(C_k, D_k, Y_{k-1}, \mu_{k-1}) - \langle Y_{k-1}, D_k - C_k W^{-1} \rangle - \frac{\mu_{k-1}}{2} \|D_k - C_k W^{-1}\|_F^2, \end{aligned}$$

which, by using the definition of Y_k and (13), can be further rewritten into

$$\begin{aligned} & \|XW - C_k\|_F^2 + \tau\|D_k\|_* \\ &= L(C_k, D_k, Y_{k-1}, \mu_{k-1}) - \langle Y_{k-1}, \frac{1}{\mu_{k-1}}(Y_k - Y_{k-1}) \rangle - \frac{\mu_{k-1}}{2} \left\| \frac{1}{\mu_{k-1}}(Y_k - Y_{k-1}) \right\|_F^2 \\ &\leq f_\infty + \frac{1}{2\mu_{k-1}} (\|Y_{k-1}\|_F^2 - \|Y_k\|_F^2). \end{aligned} \tag{14}$$

Next, by using triangle inequality we get

$$\begin{aligned} & \|XW - C_k\|_F^2 + \tau\|D_k\|_* \\ &\geq \|XW - D_k W\|_F^2 + \tau\|D_k\|_* - \|C_k - D_k W\|_F^2 \\ &\geq f_\infty - \left\| \frac{1}{\mu_{k-1}}(Y_{k-1} - Y_k)W \right\|_F^2 \\ &= f_\infty - \frac{1}{\mu_{k-1}^2} \|(Y_{k-1} - Y_k)W\|_F^2. \end{aligned} \tag{15}$$

Combining (14) and (15), we obtain the desired result. ■

References

- R. Basri and D. Jacobs. Lambertian reflection and linear subspaces. *IEEE Transaction on Pattern Analysis and Machine Intelligence*, 25(3):218–233, 2003.
- T. Bouwmans. Traditional and recent approaches in background modeling for foreground detection: An overview. *Computer Science Review*, 11–12:31 – 66, 2014.
- T. Bouwmans, A. Sobral, S. Javed, S. K. Jung, and E.-H. Zahzah. Decomposition into low-rank plus additive matrices for background/foreground separation: A review for a comparative evaluation with a large-scale dataset. *Computer Science Review*, 2016. URL [//www.sciencedirect.com/science/article/pii/S1574013715300459](http://www.sciencedirect.com/science/article/pii/S1574013715300459).
- S. Boyd, N. Parikh, E. Chu, B. Peleato, and J. Eckstein. Distributed optimization and statistical learning via the alternating direction method of multipliers. *Foundations and Trends in Machine Learning*, 3(1):1–122, 2011.
- S. Brutzer, B. Hoferlin, and G. Heidemann. Evaluation of background subtraction techniques for video surveillance. In *IEEE Computer Vision and Pattern Recognition*, pages 1937–1944, 2011.

- A. M. Buchanan and A. W. Fitzgibbon. Damped Newton algorithms for matrix factorization with missing data. In *IEEE Computer Vision and Pattern Recognition*, volume 2, pages 316–322, 2005.
- J. Cai, E. J. Candès, and Z. Shen. A singular value thresholding algorithm for matrix completion. *SIAM Journal on Optimization*, 20:1956–1982, 2010.
- E. J. Candès and Y. Plan. Matrix completion with noise. *Proceedings of the IEEE*, 98(6):925–936, 2009.
- E. J. Candès, X. Li, Y. Ma, and J. Wright. Robust principal component analysis? *Journal of the Association for Computing Machinery*, 58(3):11:1–11:37, 2011.
- A. Dutta and X. Li. On a problem of weighted low-rank approximation of matrices. *SIAM Journal on Matrix Analysis and Applications*, 38(2):530–553, 2017.
- C. Eckart and G. Young. The approximation of one matrix by another of lower rank. *Psychometrika*, 1(3):211–218, 1936.
- A. Eriksson and A. v. d. Hengel. Efficient computation of robust weighted low-rank matrix approximations using the ℓ_1 norm. *IEEE Transactions on Pattern Analysis and Machine Intelligence*, 34(9):1681–1690, 2012.
- A. Georghiadis, P. Belhumeur, and D. Kriegman. From few to many: illumination cone models for face recognition under variable lighting and pose. *IEEE Transaction on Pattern Analysis and Machine Intelligence*, 23(6):643–660, 2001.
- I. T. Jolliffe. *Principal component analysis*. Springer-Verlag, second edition, 2002.
- L. Li, W. Huang, I. H. Gu, and Q. Tian. Statistical modeling of complex backgrounds for foreground object detection. *IEEE Transaction on Image Processing*, 13(11):1459–1472, 2004.
- Z. Lin, M. Chen, and Y. Ma. The augmented lagrange multiplier method for exact recovery of corrupted low-rank matrices. 2010. URL <https://arxiv.org/abs/1009.5055>.
- J. H. Manton, R. Mehony, and Y. Hua. The geometry of weighted low-rank approximations. *IEEE Transactions on Signal Processing*, 51(2):500–514, 2003.
- I. Markovsky. *Low-rank approximation: algorithms, implementation, applications*. Communications and Control Engineering. Springer, 2012.
- I. Markovsky, J. C. Willems, B. De Moor, and S. Van Huffel. *Exact and approximate modeling of linear systems: a behavioral approach, Number 11 in Monographs on Mathematical Modeling and Computation*. SIAM, 2006.
- T. Okatani and K. Deguchi. On the Wiberg algorithm for matrix factorization in the presence of missing components. *International Journal of Computer Vision*, 72(3):329–337, 2007.

- N. Oliver, B. Rosario, and A. Pentland. A bayesian computer vision system for modeling human interactions. In *International Conference on Computer Vision Systems*, pages 255–272, 1999.
- O. Oreifej, X. Li, and M. Shah. Simultaneous video stabilization and moving object detection in turbulence. *IEEE Transaction on Pattern Analysis and Machine Intelligence*, 35(2):450–462, 2013.
- A. Sobral and A. Vacavant. A comprehensive review of background subtraction algorithms evaluated with synthetic and real videos. *Computer Vision and Image Understanding*, 122:4 – 21, 2014.
- N. Srebro, J. D. M. Rennie, and T. S. Jaakkola. Maximum-margin matrix factorization. *Advances in Neural Information Processing Systems*, 17:1329–1336, 2005.
- N. S. Srebro and T. S. Jaakkola. Weighted low-rank approximations. In *20th International Conference on Machine Learning*, pages 720–727, 2003.
- M. Tao and X. Yuan. Recovering low-rank and sparse components of matrices from incomplete and noisy observations. *SIAM Journal on Optimization*, 21:57–81, 2011.
- K. Usevich and I. Markovsky. Variable projection methods for affinely structured low-rank approximation in weighted 2-norms. *Journal of Computational and Applied Mathematics*, 272:430–448, 2014a.
- K. Usevich and I. Markovsky. Optimization on a grassmann manifold with application to system identification. *Automatica*, 50(6):1656–1662, 2014b.
- Z. Wang, A. C. Bovik, H. R. Sheikh, and E.P. Simoncelli. Image quality assessment: from error visibility to structural similarity. *IEEE Transaction on Image Processing*, 13(4):600–612, 2004.
- G.A. Watson. Characterization of the subdifferential of some matrix norms. *Linear Algebra and its Applications*, 170:33–45, 1992.
- T. Wiberg. Computation of principal components when data are missing. In *Proceedings of the Second Symposium of Computational Statistics*, pages 229–336, 1976.
- J. Wright, Y. Peng, Y. Ma, A. Ganesh, and S. Rao. Robust principal component analysis: exact recovery of corrupted low-rank matrices by convex optimization. *Advances in Neural Information Processing systems*, 22:2080–2088, 2009.